Phosphoregulation of the budding yeast EB1 homologue Bim1p by Aurora/Ipl1p

Tomasz Zimniak, Katharina Stengl, Karl Mechtler, and Stefan Westermann

Research Institute of Molecular Pathology, 1030 Vienna, Austria

EB1 (end binding 1) proteins have emerged as central regulators of microtubule (MT) plus ends in all eukaryotes, but molecular mechanisms controlling the activity of these proteins are poorly understood. In this study, we show that the budding yeast EB1 protein Bim1p is regulated by Aurora B/Ipl1p-mediated multisite phosphorylation. Bim1p forms a stable complex with Ipl1p and is phosphorylated on a cluster of six Ser residues in the flexible linker connecting the calponin homology (CH) and EB1 domains. Using reconstitution of plus end tracking in vitro and total internal reflection fluorescence microscopy, we show that dimerization of Bim1p and the presence of the linker domain are both required for efficient tip tracking and that linker phosphorylation removes Bim1p from static and dynamic MTs. Bim1 phosphorylation occurs during anaphase in vivo, and it is required for normal spindle elongation kinetics and an efficient disassembly of the spindle midzone. Our results define a mechanism for the use and regulation of CH domains in an EB1 protein.

Introduction

Microtubules (MTs) are highly dynamic polymers formed by a cylindrical assembly of αβ-tubulin subunits that have essential functions for intracellular transport, chromosome segregation, and cellular architecture. Several MT-associated proteins regulate their dynamics and interactions and help to organize the MT cytoskeleton. An important subgroup among MT-associated proteins is constituted by the plus end–tracking proteins (+TIPs), which are characterized by their preferential association with growing MT plus ends in vivo. +TIPs are highly conserved among all eukaryotes and they can be divided into different subfamilies, including the DIS/chTOG family of XMAP215-like proteins, the CLIP-170 or CLASP-related families, spectraplakins, and, finally, the EB1 (end binding 1) family of MT end–binding proteins (for reviews see Akhmanova and Hoogenraad, 2005; Akhmanova and Steinmetz, 2008). EB1 proteins have emerged as key regulators of MT plus ends in all eukaryotes (Vaughan, 2005). They contain an N-terminal calponin homology (CH) domain, which displays MT-binding activity and is part of various tubulin- or actin-binding molecules (Hayashi and Ikura, 2003; Slep and Vale, 2007). The following C-terminal coiled-coil mediates homodimerization and is followed by a four-helix bundle (EB1 homology domain), which is critical for the tethering of cargo proteins to EB1 (Honnappa et al., 2005; Slep et al., 2005). Although crystal structures of the individual CH domain and the C-terminal cargo-binding domain have been solved, the spatial organization of these domains in the context of a full-length EB1 molecule remains unknown. Two recent studies of the *Schizosaccharomyces pombe* EB1 homologue Mal3 have provided some basic insights into the function of EB1 proteins. Using an EM approach, Sandblad et al. (2006) have investigated the decoration of stabilized MTs by Mal3 and found that the protein preferentially associates with the lattice seam of the MTs, the structurally most labile part of the polymer. Thus, it may act as a "molecular zipper" supporting the stabilization of the closing lattice seam (Sandblad et al., 2006; Vitre et al., 2008). In a different approach, Bieling et al. (2007) have reconstituted the interaction of three *S. pombe* +TIPs with dynamic MTs in vitro. Notably, only the EB1 homologue Mal3p had an intrinsic ability to track the MT end and was sufficient to localize the kinesin Tea1p and the CLIP-170 protein Tip1p to growing ends in vitro (Bieling et al., 2007). Despite this progress, important questions concerning EB1-related proteins have remained unanswered. For example, what is the molecular mechanism by which these proteins bind to the MT lattice and to the growing end? Moreover, how does the cell

Correspondence to Stefan Westermann: westermannn@imp.ac.at

Abbreviations used in this paper: CH, calponin homology; MT, microtubule; SEC, size exclusion chromatography; TEV, tobacco etch virus; +TIP, plus end–tracking protein; TIRF, total internal reflection fluorescence; WT, wild type.

The Rockefeller University Press $30.00
J. Cell Biol. Vol. 186 No. 3 379–391
www.jcb.org/cgi/doi/10.1083/jcb.200901036

regulate EB1 activity to control the dynamics and transport of proteins to plus ends? Because EB1 proteins constitute the center of extensive +TIP networks and control the association of many proteins with plus ends, they are particularly important targets for regulatory mechanisms (Lansbergen and Akhmanova, 2006).

Plus ends establish the contact of MTs to various cellular structures, among them the kinetochore, a complex assembly of proteins on centromeric DNA which mediates the attachment of chromosomes to the mitotic and meiotic spindle (Westermann et al., 2007; Cheeseman and Desai, 2008; Tanaka and Desai, 2008). Regulation of kinetochore–MT attachments is particularly important in the process of biorientation, i.e., the pathway by which the cell ensures that duplicated sister chromatids are connected to opposite spindle poles (Tanaka et al., 2005). In addition, the MT plus ends of interpolar MTs are bundled to form the spindle midzone, which is required for proper spindle elongation (Khmelinskii et al., 2007) and cytokinesis (Norden et al., 2006). The mitotic kinase Aurora B is thought to be critical for the regulation of MT plus ends in both of these cellular situations. In the process of kinetochore biorientation, Aurora B phosphorylates kinetochore components to release improper attachments (Cheeseman et al., 2002; Ciferri et al., 2008), and during anaphase, Aurora B localizes to the spindle midzone, where it is involved in timely spindle disassembly (Buvelot et al., 2003). To understand how Aurora B performs its critical functions, it is essential to identify all relevant downstream targets and elucidate their mechanism of regulation.

In this study, we identify the budding yeast EB1 homologue Bim1p as an Ipl1 substrate and provide molecular insights into its regulation. Biochemical analysis has revealed that Bim1p directly associates with the Ipl1p kinase and, upon activation by Sli15p, becomes phosphorylated on a cluster of six sites in the flexible linker domain. Our analysis indicates that the Bim1p linker domain is critical for MT binding, autonomous plus end tracking, and phosphoregulation of this EB1 family member.

Results

Bim1p is phosphorylated by the Ipl1–Sli15 complex at the linker domain

To analyze the protein–protein interactions and posttranslational modifications of the budding yeast EB1 homologue Bim1p, we constructed a strain in which the endogenous *BIM1* gene was tagged at the C terminus with a tandem affinity tag. The protein was purified from yeast extracts of logarithmically growing cells, and the preparation was analyzed after in-solution digest by mass spectrometry (Fig. 1 A). Under our stringent purification conditions (300 mM KCl), the budding yeast adenomatous polyposis coli homologue Kar9p, a known interaction partner of Bim1p with a role in orienting the yeast spindle (Hwang et al., 2003), was copurified. In addition, we mapped a total of six Bim1 phosphorylation sites. Interestingly, the identified sites (Ser139, -148, -149, -165, -166, and -176) were not randomly distributed throughout the molecule but clustered in a region of 40 aa in the flexible linker region connecting the well-conserved CH and EB1-like domains (Fig. 1 B). Closer inspection of the phosphorylation sites revealed that most of them contained a consensus sequence targeted by the Aurora B kinase (Cheeseman et al., 2002), suggesting that Bim1p may be an Ipl1p substrate. To determine whether Bim1p is indeed phosphorylated by Ipl1/Aurora B, we expressed and purified full-length Bim1p from *Escherichia coli*, phosphorylated the protein with bacterially expressed Ipl1p in complex with its activator protein Sli15p, and analyzed the products of the kinase reaction by mass spectrometry. We found that precisely the same six phosphorylation sites we mapped in vivo were phosphorylated by purified Ipl1–Sli15 complex in vitro (Fig. 1 B). To further validate the phosphorylation sites, Bim1p variants in which the six mapped phosphorylation sites were either mutated to Ala to prevent phosphorylation ($Bim1^{6A}$) or mutated to aspartate to mimic constitutive phosphorylation ($Bim1^{6D}$) were expressed and purified from bacteria. Although wild-type (WT) Bim1p ($Bim1p^{WT}$) was an excellent substrate for Ipl1–Sli15 in vitro, changing the mapped phosphorylation sites to Ala or Asp prevented phosphorylation almost completely, demonstrating that the phosphorylation is highly specific for the mapped residues (Fig. 1 C). We also compared the efficiency of Bim1p phosphorylation either by Ipl1p alone or by Ipl1p and Sli15p. Although phosphorylation of Bim1p by Ipl1 alone was barely detectable under standard kinase assay conditions, the addition of Sli15p led to rapid phosphorylation (Fig. S1). Thus, effective phosphorylation of Bim1p by Ipl1p depends on the presence of Sli15p. Collectively, these results establish that Bim1p is a target of Ipl1p and that phosphorylation occurs on a cluster of six Ser residues located in the flexible linker region.

Bim1p forms a stable complex with Ipl1p via its C-terminal domain

Because Bim1p is phosphorylated by Ipl1p, we next explored which protein segments are important for mediating kinase–substrate interactions. A series of Bim1p N- and C-terminal truncation mutants were expressed, purified as GST fusion proteins, and tested for interaction with purified Ipl1–Sli15 complex in pull-down assays. We found that Ipl1–Sli15 could bind to Bim1p and that the interaction required the presence of the C-terminal residues 185–344 encompassing the EB1 homology domain, which is required for the binding of other cargo molecules to EB1 family members (Fig. 1 D and Fig. S2). The association between Bim1p and the Ipl1 complex was not affected by the phosphorylation status of Bim1p, as the phosphomimicking $Bim1^{6D}$ mutant could interact effectively with Ipl1–Sli15. Furthermore, we observed that Bim1p can interact with Ipl1p also in the absence of Sli15p (Fig. S2). The Bim1–Ipl1 interaction was very robust and could be detected by analytical size exclusion chromatography (SEC) under physiologically relevant salt concentrations of 100 mM KCl (Fig. 1 E). Interestingly, upon Ipl1p binding, the elution position of Bim1p was shifted toward a smaller Stokes radius, suggesting that interaction with Ipl1p stabilized a more compact conformation of the Bim1 molecule. In further support of a direct association, a recent genome-wide two-hybrid analysis

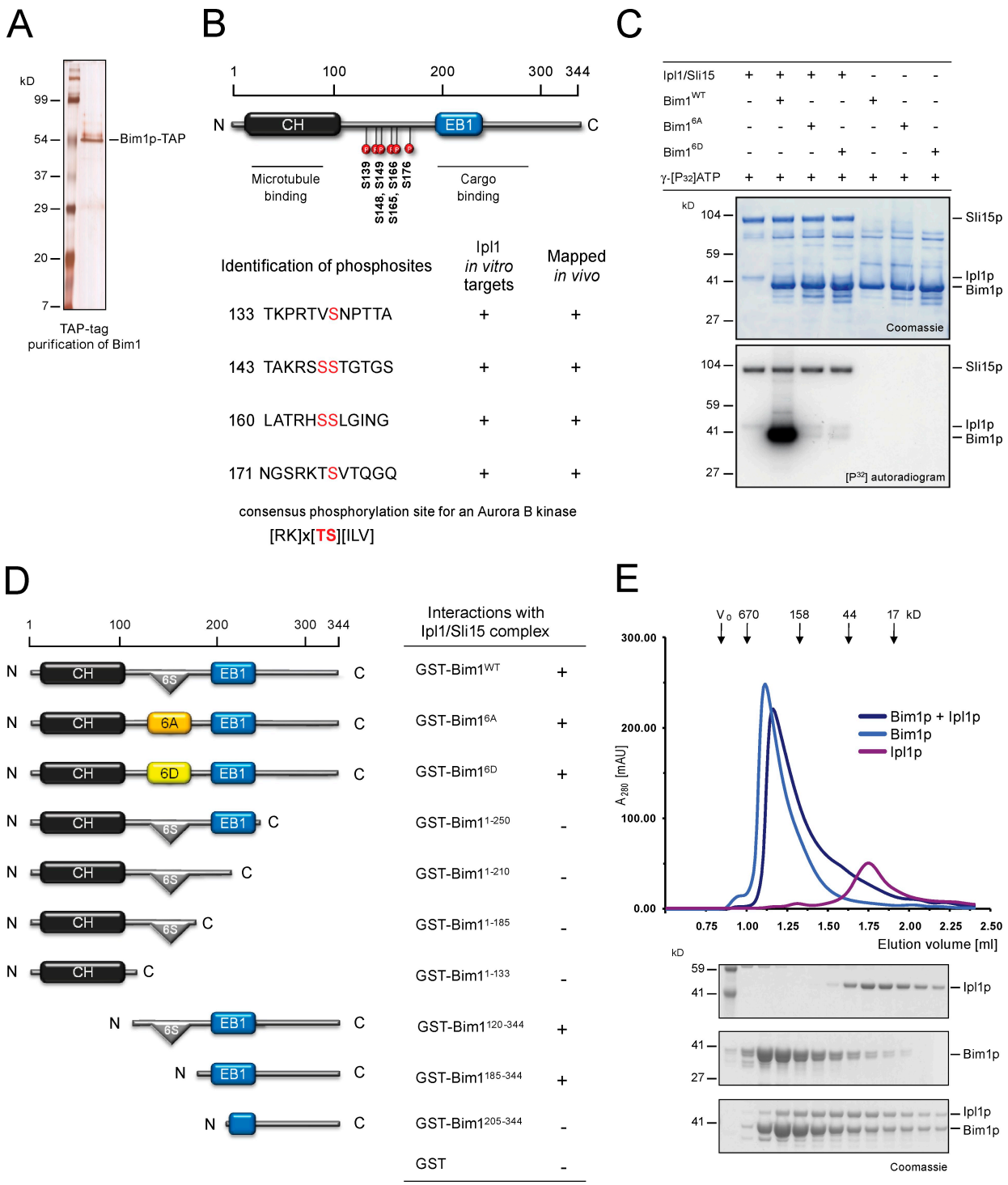

Figure 1. **Bim1p is phosphorylated by the Ipl1–Sli15 complex.** (A) Silver-stained gel of purified *Bim1–S-Tag-TEV-ZZ* from yeast extracts. TAP, tandem affinity purification. (B) Schematic representation of phosphorylation sites found after purification of Bim1p from yeast extracts and after in vitro phosphorylation of recombinant Bim1p with purified Ipl1–Sli15 complex. The phosphorylation sites cluster in the flexible linker region connecting the conserved CH and EB1 domains. (C) Validation of the mapped Bim1p phosphorylation sites. Recombinant Bim1p^{WT} and mutants either preventing (6A) or mimicking (6D) Ipl1 phosphorylation were phosphorylated with the Ipl1–Sli15 complex in vitro. Note the elimination of phosphorylation upon changing the mapped phosphorylation sites. (D) Mapping the Bim1 interaction with the Ipl1–Sli15 complex. Different N- and C-terminal truncations of Bim1p were expressed as GST fusion proteins in *E. coli* and used in pull-down assays with His6-tagged recombinant Ipl1–Sli15 complex in vitro. Binding to Ipl1–Sli15 depends on the C-terminal domain of Bim1p. (E) Analytical SEC of Bim1p and Ipl1p alone or in combination indicates the formation of a stable complex between the two proteins.

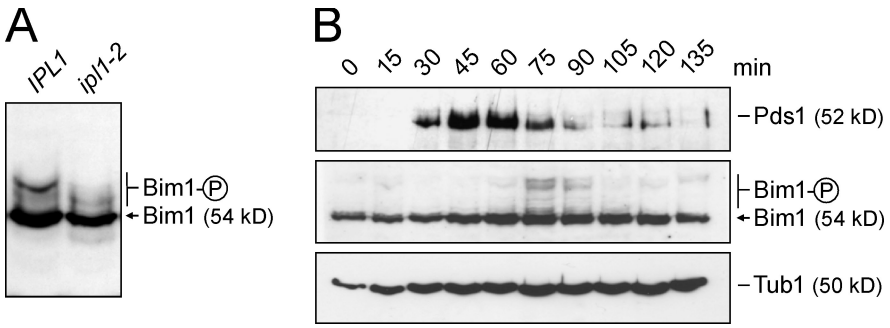

Figure 2. **Bim1 phosphorylation occurs during anaphase in vivo.** (A) Western blot analysis of Bim1 phosphorylation in a WT and in an *ipl1-2* background. SDS-PAGE was performed in the presence of 30 µM Mn^{2+} Phos-tag. Note the elimination of the slower migrating form after the shift to the restrictive temperature of an *ipl1-2* mutant. (B) Time course of Bim1 phosphorylation in an α factor arrest/release experiment. Note that the slower migrating Bim1 forms are detected after degradation of the yeast securin Pds1p. The circled P represents the phosphorylated form of the protein.

identified interactions between Bim1 and Ipl1–Sli15 (Wong et al., 2007).

We tested the effect of the multisite phosphorylated linker on the overall structure of Bim1p. We first compared the hydrodynamic properties of WT and phosphomimicking Bim1p proteins. $Bim1p^{WT}$ elutes remarkably early during SEC with a Stokes radius of 58 Å, suggesting a highly elongated shape of the dimeric molecule. However, the elution peak of the phosphomimicking $Bim1^{6D}$ mutant was shifted to a later elution volume (Fig. S3 A). This different migration behavior in SEC did not correspond to the presence of dimeric versus monomeric forms, as a Bim1p variant lacking the coiled-coil dimerization motif eluted later than the 6D mutant, reflecting its monomeric nature (Fig. S4). Thus, phosphorylation of the linker domain may lead to a conformational change of the dimeric Bim1 molecule, which results in a compaction. To further analyze the consequences of linker phosphorylation, we subjected $Bim1^{WT}$, $Bim1^{6A}$, and $Bim1^{6D}$ variants to limited proteolysis using the protease chymotrypsin. Although WT and the 6A mutant showed similar degradation patterns, the digestion pattern for the 6D mutant was significantly altered, arguing for a profound conformational change exposing different cleavage sites (Fig. S3 B). Thus, full-length Bim1p is a highly elongated molecule, and linker phosphorylation by the Ipl1–Sli15 complex may trigger a conformational change that results in a more compact dimeric molecule.

Bim1p phosphorylation occurs during anaphase in vivo

To study the phosphorylation status of Bim1p in vivo, we analyzed the pattern of epitope-tagged Bim1p by Western blotting. To enhance a potential phospho shift, SDS-PAGE was performed in the presence of the Phos-tag reagent (Kinoshita et al., 2006). In extracts derived from WT cells, Bim1p displayed slower migrating forms, which were eliminated after shifting the cells to the restrictive temperature in an *ipl1-2* mutant (Fig. 2 A). To study the timing of Bim1 phosphorylation in vivo, we synchronized cells expressing Bim1-myc and the yeast securin Pds1-myc in G1 phase of the cell cycle with α factor, released the cells, and analyzed the phosphorylation pattern by Western blotting. Interestingly, Bim1 phosphorylation was detected in a narrow time window of 15–30 min after the beginning of Pds1 degradation (Fig. 2 B). Thus, Bim1 phosphorylation depends on Ipl1 and is detected specifically during anaphase in vivo.

Multisite linker phosphorylation reduces the affinity of Bim1p for MTs

As the principal function of EB1 proteins relies on their ability to bind MTs, we next analyzed how linker phosphorylation by the Ipl1–Sli15 complex would influence the MT-binding activity of Bim1p. We compared the binding affinities of $Bim1p^{WT}$, Bim1p phosphorylated in vitro with the Ipl1–Sli15 complex, and the phosphomimicking $Bim1^{6D}$ mutant for taxol-stabilized MTs in cosedimentation assays. $Bim1p^{WT}$ displayed a robust affinity for MTs with an apparent dissociation constant (K_d) of 0.44 µM. MT binding of Bim1p phosphorylated by Ipl1–Sli15 was markedly decreased, and the apparent K_d was raised about fivefold. The phosphomimicking $Bim1^{6D}$ mutant displayed an even lower affinity for taxol-stabilized MTs (Fig. 3 A). We next asked whether Ipl1–Sli15 phosphorylation could also release Bim1p from the lattice after it had been prebound to taxol-stabilized MTs. We loaded MTs with Bim1p, incubated them with different amounts of purified Ipl1–Sli15 complex either in the absence or presence of ATP, and separated supernatant and pellet fractions after centrifugation. Only in the presence of ATP, Bim1p was removed by Ipl1–Sli15 from the pellet fraction into the supernatant (Fig. 3 B). Thus, Ipl1–Sli15-mediated phosphorylation of the Bim1p linker domain decreases the affinity for taxol-stabilized MTs in vitro and removes prebound Bim1p from the MT lattice.

To analyze the consequences of phosphorylation on Bim1p binding to MTs in vivo, we integrated $Bim1^{WT}$, $Bim1^{6A}$, and $Bim1^{6D}$ variants fused with their C termini to 3× GFP into yeast. We expressed these Bim1p variants under their own promoter in a strain lacking endogenous *BIM1* and visualized them by fluorescence live cell microscopy. Western blotting indicated that the Bim1 variants were expressed in similar amounts (Fig. 3 D). $Bim1^{WT}$–3× GFP showed a typical localization pattern with individual dots corresponding to MT plus ends and a prominent localization to the spindle midzone. The localization pattern of the 6A mutant appeared similar, although the spindle midzone seemed to be more prominently stained than in the WT control. However, the phosphomimicking 6D mutant displayed only very weak spindle staining, the cytoplasmic background signal was stronger, and only weakly fluorescent Bim1p dots remained visible (Fig. 3 C), suggesting that constitutive phosphorylation of the linker domain also impairs binding of Bim1p to MTs in vivo.

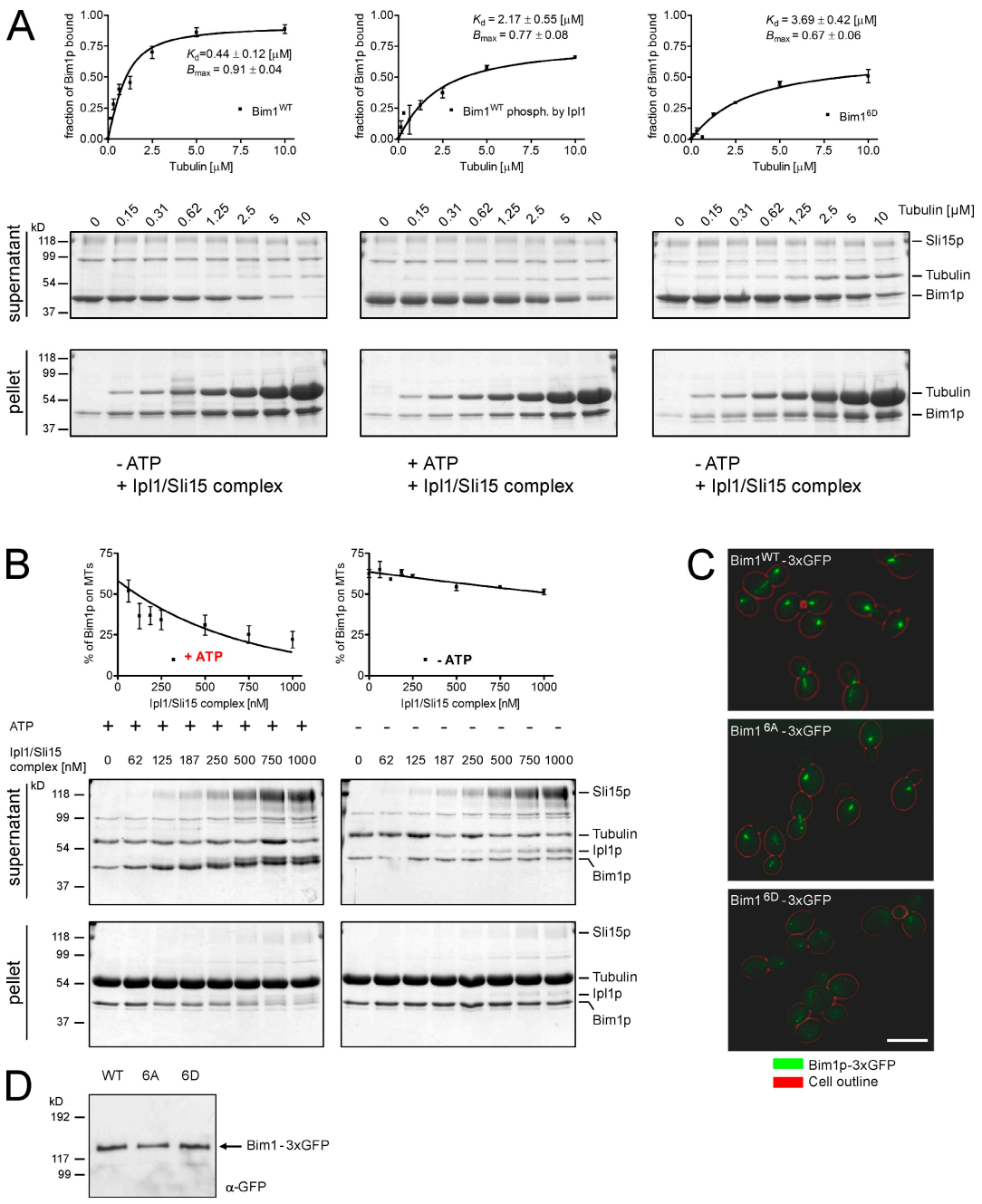

Figure 3. **Regulation of Bim1p MT binding by multisite linker phosphorylation.** (A) Equal amounts (1 μM) of Bim1^{WT}, Bim1^{WT} phosphorylated with Ipl1–Sli15, and the phosphomimicking Bim1^{6D} mutant were incubated with increasing amounts of taxol-stabilized MTs (0–10 μM). Bim1p bound to MTs was separated from the unbound fraction by ultracentrifugation, and the amount of Bim1p in the supernatant and pellet was quantified. The binding affinity curves represent averaged data from three independent experiments. (B) Bim1^{WT} was bound to 2.5 μM MTs in the presence or absence of ATP. Increasing concentrations of the Ipl1–Sli15 complex were added, the binding reaction was centrifuged, and the supernatant and pellet fractions were separated and analyzed by SDS-PAGE. The top panel displays the quantification from two independent experiments. (A and B) Error bars denote standard error of the mean. (C) Bim1^{WT}, Bim1^{6A}, and Bim1^{6D} variants were fused to 3× GFP, expressed as the sole source of Bim1p in yeast, and visualized by live cell microscopy. Examples of large-budded yeast cells are shown. Note the faint spindle staining of the 6D mutant. (D) Bim1^{WT}, Bim1^{6A}, and Bim1^{6D} mutants are expressed at similar levels, as indicated by anti-GFP Western blotting. Bar, 6 μm.

CH and linker domains synergistically enhance MT binding of Bim1p

The MT-binding activity of EB1-like proteins had previously been assigned to the CH domain (Hayashi and Ikura, 2003). However, our surprising finding that phosphorylation of the linker region substantially influences the binding of Bim1p to MTs prompted us to further investigate the mechanism of MT binding by Bim1p. To establish the molecular requirements for MT binding more rigorously, we constructed, expressed, and purified eight Bim1p variants encompassing different combinations of CH, linker, and dimerization domains as C-terminal EGFP fusion proteins (Fig. 4, A and B; and Fig. S5). This

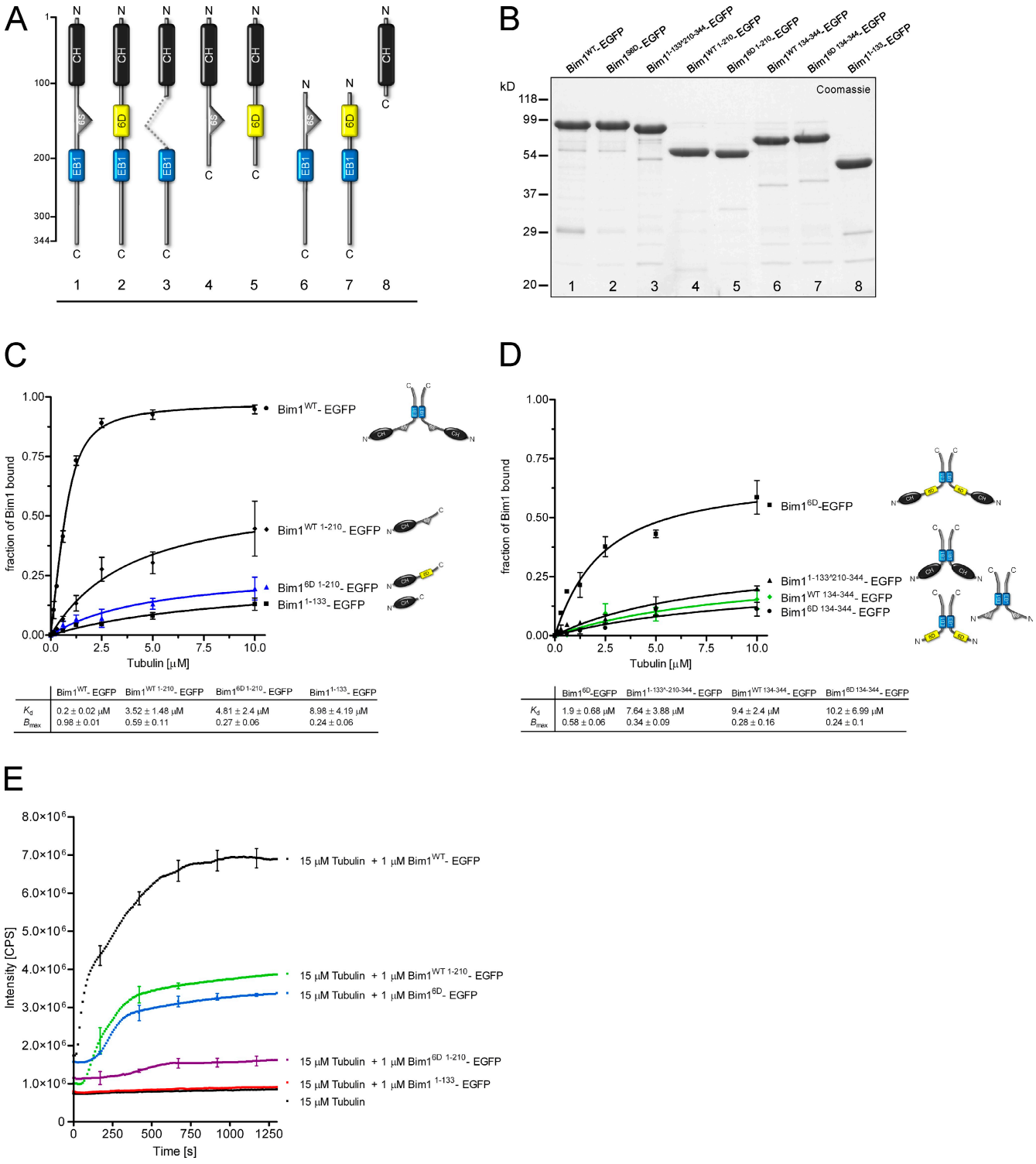

	Bim1WT- EGFP	Bim1WT 1-210- EGFP	Bim16D 1-210- EGFP	Bim11-133- EGFP
K_d	0.2 ± 0.02 μM	3.52 ± 1.48 μM	4.81 ± 2.4 μM	8.98 ± 4.19 μM
B_{max}	0.98 ± 0.01	0.59 ± 0.11	0.27 ± 0.06	0.24 ± 0.06

	Bim16D-EGFP	Bim11-133^210-344- EGFP	Bim1WT 134-344- EGFP	Bim16D 134-344- EGFP
K_d	1.9 ± 0.68 μM	7.64 ± 3.88 μM	9.4 ± 2.4 μM	10.2 ± 6.99 μM
B_{max}	0.58 ± 0.06	0.34 ± 0.09	0.28 ± 0.16	0.24 ± 0.1

Figure 4. **Molecular dissection of MT binding by Bim1p.** (A) Cartoons of Bim1 variants (WT or mutants lacking the CH, flexible linker, or dimerization domain) expressed as EGFP fusion proteins in *E. coli*. (B) Coomassie-stained gel of the respective Bim1 variants. (C) 1 μM of purified Bim1p constructs was subjected to MT binding and centrifuged. The amount of Bim1p bound to MTs was measured fluorometrically, and averaged data from three experiments were plotted as binding affinity curves. The graph compares the binding affinities of dimeric versus monomeric Bim1p variants. (D) The binding affinities of different dimeric Bimp1 constructs are compared. K_d and B_{max} values for the different constructs are summarized in the table. (E) Light-scattering experiment showing the effects of Bim1 variants on the kinetics of tubulin polymerization. (C–E) Error bars denote standard error of the mean.

allowed us to analyze the MT-binding activities in a fluorescence-based cosedimentation assay (see Materials and methods). We first tested the MT-binding activities of monomeric versus dimeric Bim1 variants (Fig. 4 C). Full-length Bim1-EGFP (residues 1–344) bound to MTs with an apparent K_d of 0.2 μM. In contrast, a monomeric construct encompassing the CH and the linker domain but lacking the coiled-coil dimerization motif (residues 1–210) showed a much lower affinity for

taxol-stabilized MTs, and the K_d was raised nearly 20-fold to 3.5 μM. Multisite phosphorylation by Ipl1p further lowered the affinity of this construct for MTs to 4.8 μM ($Bim1^{6D\ 1–210}$). Finally, a construct containing only the CH domain fused to EGFP ($Bim1^{1–133}$) bound to MTs but only weakly, with an apparent K_d of 8.9 μM.

In the next series of experiments, we compared the MT-binding activities of different dimeric Bim1 constructs (Fig. 4 D). Compared with full-length Bim1p, a variant lacking the CH domains ($Bim1^{134–344}$) displayed an ∼40-fold lower MT-binding activity. Multisite phosphorylation of the linker domain further reduced the MT affinity of this construct. Interestingly, a dimeric Bim1 variant that contained both CH domains but lacked the flexible linker residues ($Bim1^{1–133\text{^}210–344}$) displayed an MT-binding activity that was as low as the construct missing the CH domains.

We tested the effects of our engineered Bim1p constructs on tubulin polymerization using a light-scattering assay. As expected, full-length Bim1p strongly promoted MT assembly in vitro. Under the same experimental conditions, the phosphomimicking 6D mutant and the monomeric Bim1 variant containing the CH and linker domain both displayed a strongly reduced ability to promote tubulin polymerization. A construct encompassing the CH domain alone was completely ineffective in promoting polymerization (Fig. 4 E). To exclude the possibility that the observed effects are caused by the fusion with EGFP, we repeated these experiments with an additional set of constructs that contained EGFP connected by a C-terminal flexible 36-aa linker and did not see any significant changes in protein behavior (unpublished data).

Collectively, these results demonstrate that the CH domain of Bim1p is necessary but not sufficient for MT binding of the molecule. The flexible linker region contributes significantly to MT binding, and CH and linker domains synergistically allow MT binding of the full-length Bim1p molecule.

In vitro reconstitution of Bim1p plus end tracking and regulation

In the cell, Bim1p exerts its functions on dynamic MTs. Thus, we aimed to reconstitute and directly visualize the interaction of Bim1p with dynamic MTs in vitro. To this end, we modified a microscopy flow cell assay, which was previously used to analyze the dynamics of the Dam1 ring complex (Westermann et al., 2006). We adhered short, brightly labeled, biotinylated MT seeds that had been stabilized with the slowly hydrolyzing GTP analogue GMPCPP (guanosine 5′-[α,β-methylene]triphosphate) to the surface of a coverslip via a biotin–streptavidin interaction (Fig. 5 A). After washing away any unbound seeds, dimly labeled free tubulin at a concentration of 15 μM was introduced. MTs were visualized at 30°C using total internal reflection fluorescence (TIRF) microscopy to eliminate the background fluorescence generated by unincorporated labeled tubulin dimers. Under these conditions, individual MTs grew from the stable seeds and displayed dynamic instability; i.e., phases of growth were followed by rapid disassembly before another growth phase started. A similar experimental setup has recently been used by Bieling et al. (2007) to investigate the properties of the *S. pombe* EB1 homologue Mal3p.

We first analyzed the behavior of full-length $Bim1p^{WT}$ in the in vitro tracking assay: 70 nM Bim1-EGFP was added together with free tubulin into the flow chamber. Two-color time-lapse imaging demonstrated that Bim1-EGFP preferentially accumulated at MT ends during phases of growth but was rapidly lost from the MT upon disassembly (Fig. 5 C and Videos 1 and 2). Although the majority of Bim1p accumulated at growing plus ends, there was always a significant amount of Bim1p also bound to the MT lattice, which increased upon lowering the ionic strength of the solution or raising the Bim1p concentration in the assay (unpublished data). In alternative experiments, we followed the plus end tracking with Bim1p covalently conjugated to Alexa Fluor fluorophores, either via Cys or amine linkages (unpublished data). We did not observe significant differences between the Alexa Fluor conjugates and the EGFP fusion protein. Thus, we conclude that the budding yeast EB1 homologue Bim1p autonomously tracks growing MT ends in vitro.

The molecular requirements for autonomous plus end tracking have not been established in a defined in vitro system. Therefore, we tested our engineered Bim1 constructs in the in vitro tracking assay and asked whether they could associate with the MT lattice or with growing ends (Fig. 5 B). Under conditions in which $Bim1p^{WT}$ displayed robust plus end tracking (70 nM final Bim1p concentration), the monomeric variant ($Bim1^{1–210}$) only weakly associated with dynamic MTs. Raising the final concentration of $Bim1p^{1–210}$ to 1 μM yielded a faint staining all along the MT lattice, whereas a substantial Bim1 accumulation at growing ends could not be observed (Fig. 5 C and Video 3). Thus, a monomeric Bim1p variant containing the CH and the linker domain failed to plus end track in vitro. In agreement with its low MT-binding affinity in the cosedimentation assay, the dimeric Bim1 variant lacking the linker domain ($Bim1^{1–133\text{^}210–344}$) was barely visible on MTs under our imaging conditions and did not display tip-tracking activity. Thus, dimerized CH domains and the presence of the linker are both necessary for the autonomous plus end–tracking activity of Bim1p.

To visualize the effect of Ipl1–Sli15 phosphorylation, we first analyzed the interaction of Bim1p with stable MT substrates. We incubated rhodamine-labeled, taxol-stabilized MTs with Bim1p–Alexa Fluor 488 and observed the binding reaction by TIRF microscopy. Bim1p–Alexa Fluor 488 decorated taxol-stabilized MTs along their length without any observable preference for MT ends. We included purified Ipl1–Sli15 complex in the binding reaction, and during recording, we introduced ATP into the flow chamber. Within seconds after ATP addition but not after a buffer control, the Bim1p–Alexa Fluor 488 signal disappeared from taxol-stabilized MTs (Fig. 5 D and Video 4). Finally, we investigated the effect of Ipl1 phosphorylation on plus end tracking in vitro. We performed the tip-tracking assay as described in this section but now added purified Ipl1–Sli15 complex either in the presence or absence of ATP. After initial association with growing plus ends, the Bim1 signal disappeared from the plus ends as well as from the lattice. This was not the case in control assays in which either the Ipl1–Sli15 complex or ATP was omitted from the reaction (Fig. 5 E and Video 5). These results demonstrate that linker phosphorylation by Ipl1p removes Bim1p from dynamic MTs in vitro.

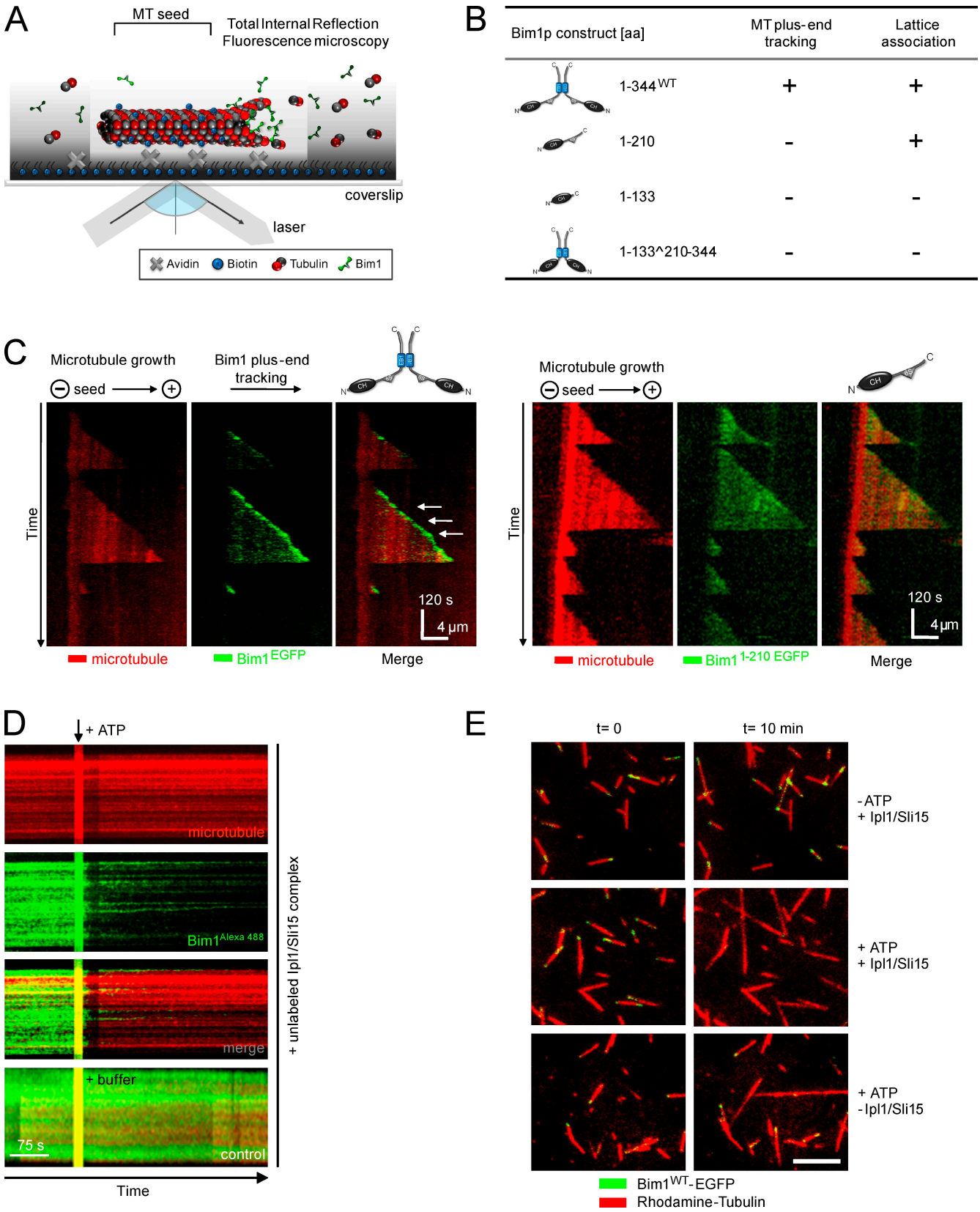

Figure 5. **Reconstitution of Bim1p MT plus end tracking in vitro using TIRF microscopy.** (A) Scheme of the experimental setup. (B) Table summarizing the ability of different Bim1 constructs for MT plus end tacking or lattice association. (C) Full-length Bim1-EGFP autonomously tracks a growing MT plus end in vitro. A kymograph representation demonstrating 70 nM Bim1p tip tracking is shown. Note that Bim1p is not found on the tips of depolymerizing MTs (left; Videos 1 and 2). Association of 1 µM of a Bim1p variant lacking the dimerization domain (Bim1p$^{1-210}$) with dynamic MTs. Note that this variant faintly stains the MT lattice but fails to accumulate at growing ends (right; Video 3). Arrows show enrichment of Bim1 on the growing MT end. (D) In a microscopy flow cell, Alexa Fluor 488–labeled Bim1p (green) was bound to rhodamine-labeled, taxol-stabilized MTs. At the indicated time, ATP was added into the

Bim1p phosphorylation affects spindle dynamics and is critical for proper midzone disassembly in vivo

As Bim1p phosphorylation occurred preferentially in anaphase, we compared the spindle elongation kinetics of WT and mutant *bim1* cells using time-lapse live cell microscopy in strains expressing GFP-tubulin. Spindle elongation in WT cells occurred with typical biphasic kinetics consisting of an initial fast and a subsequent slow phase (Fig. 6 A). In a *bim1* deletion mutant, elongation started from a shortened metaphase spindle, the rate of elongation in anaphase was reduced, and the final spindle length was decreased. The *bim1* mutant mimicking Ipl1 phosphorylation (*Bim1*^{6D}) displayed spindle elongation kinetics very similar to WT cells. In contrast, the mutant preventing Ipl1 phosphorylation (*Bim1*^{6A}) showed a faster rate of spindle elongation in both phases of anaphase B and reached an increased maximum spindle length. These results suggest that Bim1 phosphorylation is required for spindle elongation to occur with normal kinetics. As the spindles in the phosphorylation-deficient *bim1* mutant grew faster and overextended, we also analyzed the mode of spindle disassembly by following the dynamic behavior of GFP-tagged Bim1^{WT} or Bim1 phosphorylation mutants in strains expressing mCherry-tubulin. Bim1^{WT} was prominently localized to the spindle midzone in anaphase cells, and during spindle disassembly, the length of the Bim1 zone gradually decreased until only a small amount of Bim1p remained on the ends of depolymerizing spindle MTs (Fig. 6 B and Video 6). The Bim1 phosphorylation-deficient mutant displayed a different behavior: upon spindle disassembly, the length of the Bim1 midzone decreased slightly, but in contrast to WT cells, a significant amount of *Bim1*^{6A} remained on the spindle. Instead of disassembling by depolymerization, the spindle then broke, and Bim1p remained on the ends of the MTs (Fig. 6 B, right; and Video 7). In extreme cases, instead of disassembling, the spindle even started to polymerize again and was bent before finally separating (Video 8). The *Bim1*^{6D} mutant displayed only a weak signal on the spindle MTs, and the spindle disassembled efficiently (Video 9). Collectively, these results demonstrate that Bim1 phosphorylation by Ipl1 is required for efficient disassembly of the spindle midzone in vivo.

Discussion

The mitotic kinase Aurora B has an important role in regulating MT plus ends in the process of kinetochore biorientation and at the spindle midzone, but only few relevant substrates have been identified. In this study, we show that Bim1p, a member of the evolutionary conserved family of EB1 proteins, is a physiological substrate of the yeast Aurora kinase Ipl1p. In addition to characterizing Bim1's role in spindle dynamics, our study provides insights into the molecular mechanism and regulation of autonomous plus end tracking by EB1 proteins.

Functional organization of EB1 proteins

The molecular mechanisms regulating the activity of EB1 proteins have so far remained elusive. In this study, we identify the flexible linker region as the critical regulatory domain of the budding yeast EB1 homologue Bim1p (Fig. 7 A). This was unexpected, as previous work had assigned the MT-binding activity to the CH domain, and it has been speculated that the regulatory mechanisms may target this region of the molecule (Hayashi and Ikura, 2003). Among EB1 homologues, the sequence of the linker region is less well conserved than the CH and dimerization domains. However, the approximate length of the linker, its predicted unstructured nature, and its overall basic electrostatic character are common features of all EB1 proteins. A recent study suggests that the linker region may also be of critical importance for the *S. pombe* EB1 homologue Mal3, as C-terminal truncations of a monomeric Mal3 construct abolished its polymerization-promoting activity (des Georges et al., 2008). There is further evidence that the observed interaction between Bim1p and Ipl1p may be evolutionary conserved: using two-hybrid and coimmunoprecipitation analyses, a recent study identifies human Aurora B as an interaction partner of EB1 (Sun et al., 2008). Although a direct phosphorylation of EB1 by Aurora B could not be detected in vitro, which may be caused by the absence of an activator protein, there remains the possibility that either EB1 or the related proteins EB2 and -3 may be relevant physiological Aurora B targets. Furthermore, we did not obtain experimental evidence that Bim1p is regulated by autoinhibition between the CH domains and the extreme C termini, as has been proposed for EB1 (Hayashi et al., 2005). The reason may be that Bim1p is significantly larger than EB1 (344 residues compared with 268 for EB1) or that the C-terminal residues (ETF for Bim1p) differ from the sequence found in EB1 (EEY).

A common mechanism for the function and regulation of CH domains as MT-binding interfaces

With the identification of Bim1p as an Ipl1 target, it is noteworthy to point out striking similarities between its regulation of MT binding and that of the Ndc80 kinetochore complex. Both molecules exploit CH domains as part of their MT-binding interfaces (Cheeseman et al., 2006; Wei et al., 2007), yet in both cases, unstructured regions located adjacent to the globular CH domain contribute significantly to MT binding and are the target of Aurora B phosphorylation at a cluster of neighboring residues (Ciferri et al., 2008; Guimaraes et al., 2008; Miller et al., 2008). Recent cryo-EM studies describing the decoration of MTs by Ndc80/Nuf2 (Wilson-Kubalek et al., 2008) or by the *S. pombe* EB1 homologue Mal3 (des Georges et al., 2008) suggest that the CH domain nestles into a groove at the interface between tubulin dimers on the MT lattice. The N-terminal tail domain of Ndc80 and the linker domain of EB1 proteins may

flow cell. In the kymograph representation, the Bim1p signal disappears rapidly from the stable MTs; in contrast, it persists in a buffer control (Video 4). (E) In vitro tracking of Bim1p in the presence of the Ipl1–Sli15 complex. Bim1p is removed from growing MT ends when the Ipl1–Sli15 complex and ATP are present (Video 5). Bar, 5 µm.

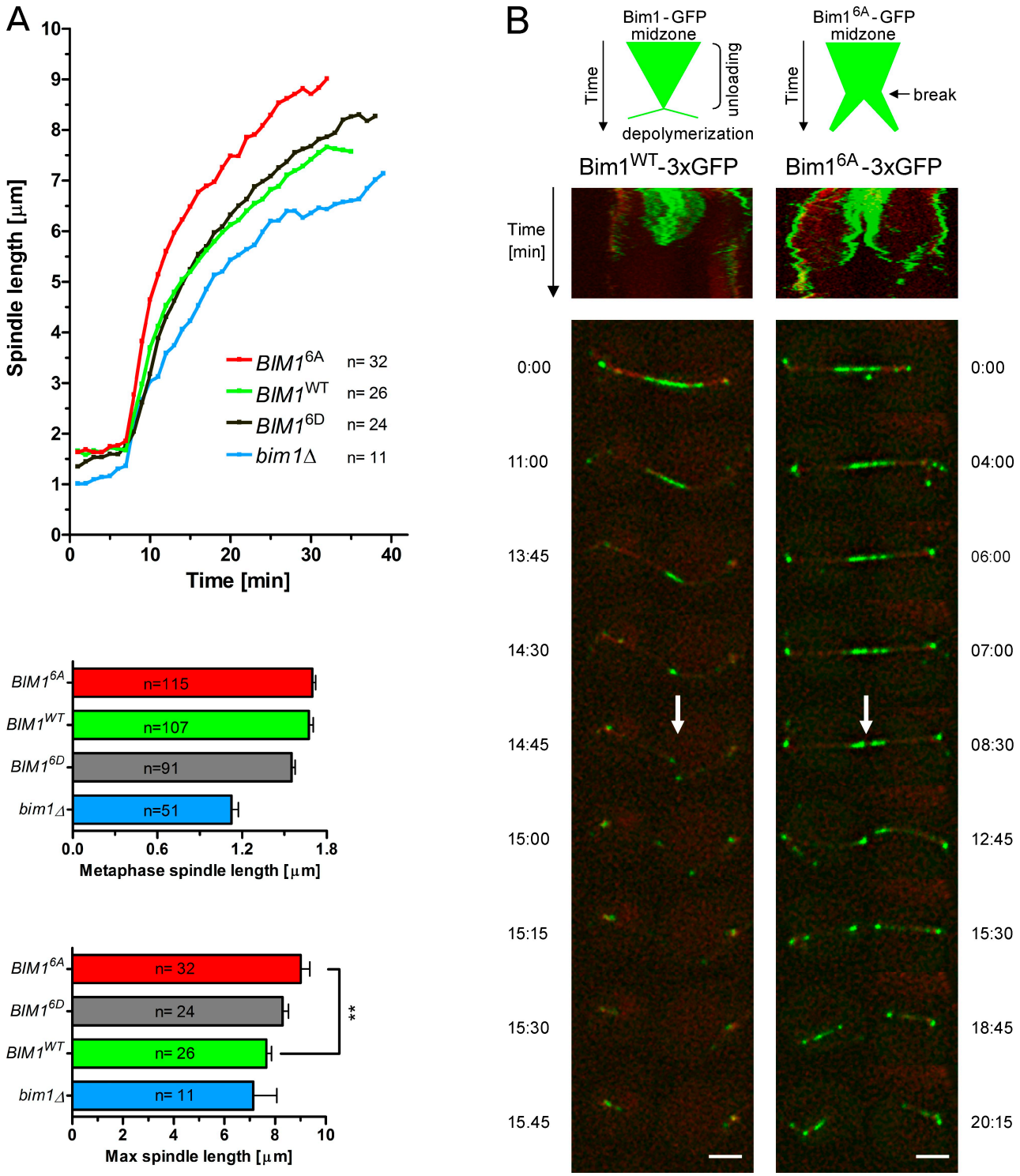

Figure 6. **Bim1 phosphorylation affects spindle dynamics and midzone disassembly in vivo.** (A) Averaged kinetics of anaphase spindle elongation in WT, *BIM1*^{6A}, *BIM1*^{6D}, and *bim1Δ* cells followed by live cell microscopy of strains expressing *GFP-TUB1*. (middle and bottom) Quantification of maximum anaphase spindle length and metaphase spindle length in the different *bim1* mutants. Error bars denote standard error of the mean. **, P = 0.0011. (B) Live cell microscopy of *BIM1–3× GFP* and *BIM1*^{6A}*–3× GFP* during spindle disassembly in strains expressing *mCherry-TUB1*. The middle panels show kymographs (space–time plots) of midzone disassembly in the WT and in the *BIM1*^{6A} background. The bottom panels show individual frames from the corresponding videos for a WT spindle (Video 6) and for the 6A mutant (Video 7). Arrows show separation of the Bim1 signal on the spindle. Bars, 3 μm.

contribute to binding by interacting with the negatively charged C-terminal tails of αβ-tubulin (E-hook). CH domains are used by a variety of molecules with very different binding partners. It seems that a general theme for their usage in MT binding is to combine them with adjacent flexible regions that have an overall positive charge. Modulating the electrostatic properties of the linker domain may be a very effective way to control the affinity for MTs. Mechanistically, there are different possibilities

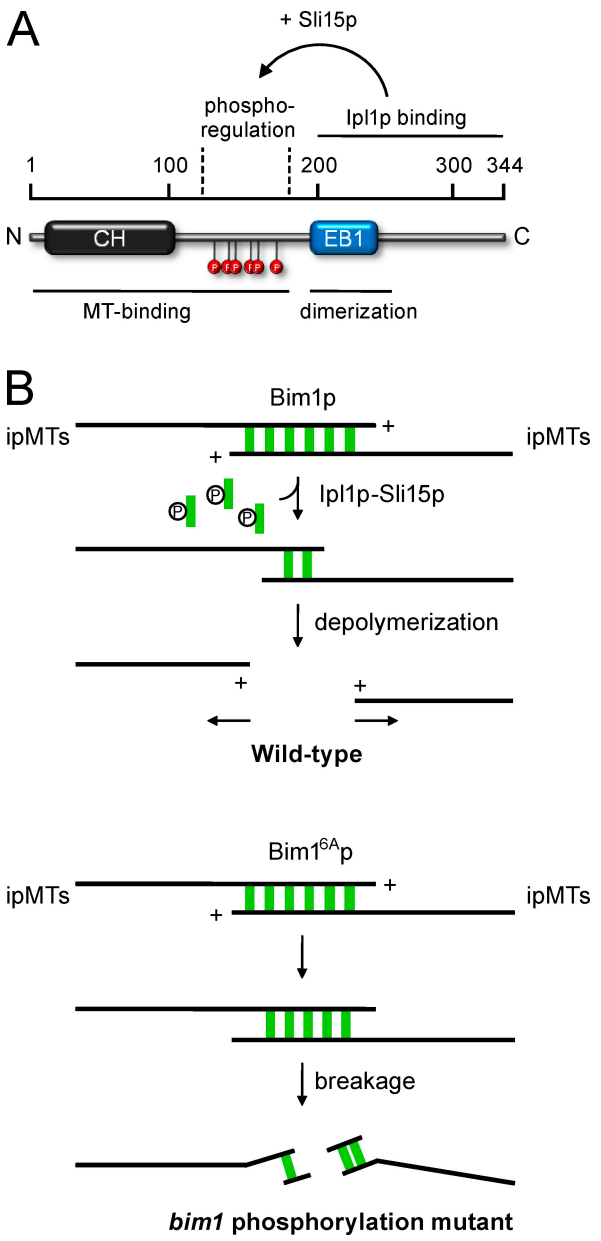

Figure 7. **Model for Bim1 phosphoregulation.** (A) Functional domains and regulation of the EB1 family member Bim1p. (B) Model for the role of Bim1 phosphorylation by Ipl1–Sli15 in the process of midzone disassembly. In a WT cell, Ipl1 phosphorylation facilitates the removal of Bim1p from the midzone and allows spindle disassembly. In a phosphorylation mutant, Bim1p persists at the spindle midzone, leading to defects in disassembly and spindle breakage. ipMT, interpolar MT.

by which this can be achieved. First, multisite phosphorylation may down-regulate the MT-binding activity that is intrinsic to the unstructured region by changing its bulk electrostatic properties (Serber and Ferrell, 2007). Second, it may change the conformation of the flexible linker region with the consequence that the CH domains are not in the optimal position for cooperative MT binding anymore. Third, cluster phosphorylation may create a negatively charged domain that could compete with tubulin for binding to the CH domains (Fig. 7 A). The observed conformational compaction of the Bim1 molecule upon multisite phosphorylation of the linker domain supports the latter two possibilities.

Establishing molecular requirements for plus end tracking

The reconstitution of MT plus end tracking in vitro using a purified system in combination with the engineering of fluorescently labeled Bim1p variants has allowed us to address the basic molecular requirements for autonomous tip tracking. We demonstrate that Bim1p, like Mal3 (Bieling et al., 2007), autonomously tracks growing MT ends in a purified system. Given the high degree of evolutionary conservation and a recent study demonstrating end tracking of *Xenopus laevis* EB1 (Bieling et al., 2008), we expect autonomous tip tracking to be a general, defining feature of all EB1 proteins. Furthermore, we show that MT-binding CH domains and even dimerized CH domains alone are not sufficient to allow effective plus end tracking of Bim1p in vitro. Instead, our results indicate that the flexible linker region has an essential role in providing full MT-binding and tip-tracking activity. The failure of a monomeric Bim1p construct to display tip tracking is not just caused by its overall lower binding affinity for MTs because even raising its concentration in the assay does not lead to a specific accumulation at MT ends. Instead, it seems that the dimeric arrangement of CH and linker domains is essential for the effective recognition of a specific structure at assembling MT ends (Bieling et al., 2007). This result agrees with in vivo observations demonstrating that artificial dimerization allows plus end tracking of various +TIPs (Slep and Vale, 2007). However, it is in contrast to a recent study demonstrating that an isolated CH domain of the human EB3 protein shows specific accumulation on growing plus ends in vitro (Komarova et al., 2009). Different properties of Bim1p versus EB3 may explain the contrasting experimental outcomes. In the future, the minimal requirements for plus end tracking will have to be investigated in more detail, and it will be interesting to see whether MT-binding proteins that have different arrangements of CH domains can display autonomous tip tracking. For example, in the Ndc80/Nuf2 head of the Ndc80 complex, the two CH domains reside very close together (Ciferri et al., 2008) and provide one common rather than two spatially separated MT-binding interfaces.

The role of Bim1 phosphorylation in vivo

What is the physiological role of Bim1 phosphorylation by Ipl1p? As judged from a mobility shift in SDS-PAGE, a fraction of Bim1p becomes phosphorylated in a narrow time window after securin degradation in mid to late anaphase. At this time, Bim1p localizes to the midzone of the anaphase spindle and is critical for its structural integrity by stabilizing the zone of overlapping MT plus ends (Gardner et al., 2008). Our results suggest that phosphorylation by Ipl1 regulates the interaction of Bim1p with the anaphase spindle. The Ipl1–Sli15 complex colocalizes with Bim1p to the spindle midzone (Khmelinskii et al., 2007), and Ipl1 kinase activity increases before spindle disassembly (Buvelot et al., 2003). Although a stable midzone is essential for proper spindle elongation, the zone of overlapping MT plus ends needs to be destabilized to allow efficient spindle disassembly in telophase. In a WT cell, the majority of Bim1 is unloaded from the spindle just before disassembly, but in the Bim1 phosphorylation mutant, this unloading process is inefficient, the midzone is hyperstable, and the spindle disassembles

by breakage rather than plus end depolymerization (Fig. 7 B). A constitutively high level of Bim1p on the spindle would also explain why the spindle overextends in the phosphorylation-deficient mutant. With an extended overlap zone, motors can act more efficiently in the fast phase of elongation, and sustained plus end polymerization will allow further extension in the slow phase. It is important to note that the *bim1* phosphorylation-deficient mutant does not precisely phenocopy the *ipl1-2* mutant, as this allele is not reported to have an effect on anaphase B kinetics (Buvelot et al., 2003). This may be explained by the presence of additional Ipl1 substrates relevant for spindle elongation such as the bundling protein Ase1p (Kotwaliwale et al., 2007). We also do not exclude additional functions for Bim1 phosphorylation and for the Bim1–Ipl1 interaction, particularly in the process of kinetochore biorientation. Additional mutants that specifically affect the interaction between Bim1p and Ipl1 will be required to clarify whether this association is critical for the regulation of MT plus ends in other cellular situations.

Materials and methods

Yeast strain construction, purification of Bim1–S-Tag–tobacco etch virus (TEV)–ZZ from yeast extracts, and mass spectrometry analysis

Yeast strains (Table S1) were constructed using standard procedures. C-terminal S-Tag-TEV-ZZ (tandem affinity purification) tags, deletions, and conditional alleles of Bim1 were constructed by PCR as described previously (Cheeseman et al., 2002). Phosphorylation site mutants were generated using QuikChange Multi Site-Directed Mutagenesis (Agilent Technologies), cloned into modified pRS303–3× GFP, and integrated into a *bim1Δ* strain. All growth experiments were conducted in YPD (YP + 2% dextrose), and tandem affinity purification tag purification was performed as described previously (Cheeseman et al., 2002). Mass spectrometry analysis was performed after in-solution digest of purified Bim1p from two independent preparations.

Cloning, expression, and purification of Bim1p variants

PCR amplified *Saccharomyces cerevisiae BIM1* ORF was ligated into pBSIIKS, modified pGEX-4T-TEV, or modified pET28a(+)-EGFP plasmids. QuikChange Multi Site-Directed Mutagenesis was used to selectively mutate serines on pBSII KS-Bim1^{WT} full length (Ser139, -148, -149, -165, -166, and -176) into alanines or aspartic acids, and mutations were verified by sequencing. GST-TEV-Bim1^{WT}, -Bim1^{6A}, and -Bim1^{6D} variants were expressed overnight at 18°C after induction with 0.1 mM IPTG. Bacteria were disrupted by sonication in the presence of protease inhibitors (Roche), and fusion proteins were purified from cell lysates using glutathione-Sepharose (GE Healthcare). Phosphate buffer A (25 mM NaH_2PO_4/Na_2HPO_4, pH 6.8, 300 mM NaCl, and 1 mM EDTA) was used for lysis, incubation, and washing of the beads. Bim1 protein was finally cleaved off the GST moiety after overnight incubation at 8°C with 0.01 mg/ml TEV protease in buffer B (25 mM NaH_2PO_4/Na_2HPO_4, pH 6.8, 150 mM NaCl, 1 mM EDTA, 0.1% Tween 20, and 1 mM DTT). The eluate was subjected to anion exchange chromatography using a HiTrapQ 1-ml column (GE Healthcare) and developed with a linear gradient. Protein concentration was determined with D_C Protein Assay kit (Bio-Rad Laboratories), and samples were frozen in the presence of 5% (vol/vol) glycerol at −80°C. 6× His–tagged Bim1-, Ipl1-, or Sli15-EGFP fusion proteins, either individually or with a flexible 36-aa linker at the fusion site (QQFFGDDSPFCQEGSPFQSSPFC-QGGQGGNGGGQQQ), were expressed under the aforementioned conditions but purified using buffer C (25 mM NaH_2PO_4/Na_2HPO_4, pH 7.5, 400 mM NaCl, and 15 mM imidazole) and Ni–nitrilotriacetic acid agarose (QIAGEN). Elution of proteins was performed with 200 mM imidazole followed by buffer exchange (25 mM NaH_2PO_4/Na_2HPO_4, pH 7.5, 150 mM NaCl, and 1 mM EDTA) using PD-10 columns (GE Healthcare).

Kinase assays

Recombinant Ipl1–Sli15 complex at a concentration of 0.1 mg/ml was incubated with Bim1p substrates in kinase buffer (25 mM Hepes, pH 7.5, 150 mM KCl, 1 mM EDTA, 4 mM $MgCl_2$, 10% glycerol, and 1 mM DTT) in the presence of γ-[P^{32}]ATP. The reaction was performed at 25°C for 30 min, and products were separated by SDS-PAGE and analyzed by autoradiography.

In vitro binding assays

5 µg of purified GST fusion Bim1 proteins was added to 30 µl glutathione-Sepharose and 10 µg of the Ipl1–Sli15 complex (precleared with the same amount of beads) in a final volume of 400 µl of binding buffer (25 mM Hepes, pH 7.5, 100 mM KCl, 3 mM $MgCl_2$, 1 mM EDTA, 10% glycerol, 0.1% NP-40, and 1 mM DTT). After incubation for 1 h at 8°C, beads were washed three times with 0.5 ml of binding buffer and analyzed by Western blotting, and kinase complex was detected with anti–5× His antibodies (QIAGEN).

Analytical SEC

The indicated Bim1 variants were diluted into gel filtration buffer (25 mM NaH_2PO_4/Na_2HPO_4, pH 6.8, 150 mM NaCl, and 1 mM EDTA) on ice for 10 min before loading onto a Superdex 200 PC 3.2/30 (GE Healthcare) or Superose 6 PC 3.2/30 column (GE Healthcare) equilibrated in gel filtration buffer. Fractions of 50 µl were collected and separated by SDS-PAGE. Proteins were stained with Coomassie Brilliant blue R250.

MT-binding assays (conventional/fluorescence based)

Binding assays were performed essentially as previously described (Cheeseman et al., 2001). Precleared Bim1^{WT}, Bim1^{WT} phosphorylated preparatively by Ipl1, and Bim1^{6D} (at 1 µM) were incubated with increasing concentrations of taxol-stabilized MTs (0–10 µM) in 25 mM Hepes, pH 7.5, 150 mM KCl, 4 mM $MgCl_2$, 1 mM EGTA, and 10% glycerol. Bim1 bound to MTs was separated from unbound fraction by ultracentrifugation. The amount of Bim1p in supernatant and pellet was quantified by densitometry of Coomassie-stained SDS-PAGE gels using ImageJ software (National Institutes of Health). To determine apparent K_d of Bim1 for MTs, data points from three independent experiments were fitted into the equation $Y = 0.5 \times \{(K_d + B_{max} + X) - [(K_d + B_{max} + X)^2 - (4B_{max}X)]^{1/2}\}$ using Prism 4.0 (GraphPad Software, Inc.), where Y is the concentration of Bim1 partitioning to the pellet with the MTs, B_{max} is the maximal fractional Bim1–MTs complex, K_d is the dissociation constant, and X is the concentration of polymeric tubulin.

In the fluorescent-based MT-binding assay, 1 µM of purified Bim1 constructs was subjected to MT binding as described in the previous paragraph and centrifuged. The amount of Bim1 bound to MTs was measured fluorometrically using a plate reader (Synergy 2; BioTek), and averaged data from three individual experiments were similarly plotted as binding affinity curves.

Light-scattering assay

8 mg/ml tubulin and 1 µM of Bim1 variants were incubated on ice in BRB80 buffer containing 1 mM GTP (in a total volume of 60 µl) and transferred into 3-mm quartz cuvettes. Right-angle light scattering of the solution was recorded every 10 s for a period of 30 min at 350 nm in a spectrofluorometer (FluoroMax4; Horiba Scientific) equilibrated to 30°C.

In vitro reconstitution of plus end tracking using TIRF microscopy

The preparation of perfusion chambers for microscopy was previously described (Westermann et al., 2006). Assay chambers were constructed using acid-washed cover glasses and silanized glass slides. Assembled chambers were first washed with miliQ water. A solution of 5 mg/ml biotinylated BSA (Vector Laboratories) was flowed in for 1 h and exchanged afterward with blocking solution containing 80 µg/ml casein, 0.1% pluronic F-127 (Sigma-Aldrich), and 1% polyethylene-block poly(ethylene glycol) (Sigma-Aldrich) in BRB80 buffer for 30 min. The chamber was then incubated with 0.3 mg/ml avidin DN (Vector Laboratories) in blocking buffer for at least 30 min. Reaction chambers were equilibrated with assay buffer (BRB80 supplemented with 150 mM KCl, 0.33 mg/ml casein, 0.5% β-mercaptoethanol, 4.5 µg/ml glucose, 200 µg/ml glucose oxidase, and 35 µg/ml catalase) and incubated with rhodamine-labeled, GMPCPP-stabilized short MT seeds for 1 min. Dynamic MT growth was initiated by flowing 15 µM of tubulin solution (containing 1 µM rhodamine-labeled tubulin) in assay buffer and visualized at 30°C using the TIRF3 microscopy system (Carl Zeiss, Inc.) operated with Axiovision software (Carl Zeiss, Inc.) and a 100× α Plan-Apochromat 1.46 NA objective. Time-lapse recordings were acquired every 5 s using an electron-multiplying charge-coupled device camera (C9100-02; Hamamatsu Photonics). For the observation of Bim1 plus end tracking, 70 nM EGFP-tagged Bim1 protein or 150 nM Bim1–Alexa Fluor 488 was included in the tubulin mix. In phosphoregulation assays, recombinant Ipl1–Sli15 complex at 0.1 mg/ml and 0.1 mM ATP were additionally included.

Live cell imaging

To quantify spindle elongation kinetics, cells were arrested with α factor, released into synthetic medium, and imaged on concanavalin A–coated culture dishes (Matek) at 30°C. z stacks (eight stacks 0.4 µm apart) were acquired at 1-min intervals on a microscope (Axiovert 200M; Carl Zeiss,

Inc.) equipped with a 100× α Plan-Apochromat 1.46 NA objective and a CoolSNAP HQ camera (Photometrics) controlled by MetaMorph software (MDS Analytical Technologies). Spindle length measurements were performed using ImageJ. Strains expressing *Bim1–3× GFP* and *mCherry-Tub1* were visualized by live cell Deltavision deconvolution microscopy (Applied Precision, LLC) on a microscope (IX-71; Olympus) controlled by SoftWoRx (Applied Precision, LLC) and equipped with a 100× Plan-Apochromat 1.4 NA objective (Olympus) and a CoolSNAP HQ camera at 25°C. z stacks (eight stacks 0.35 µm apart) were acquired at 15-s intervals, deconvoluted, and projected into 2D images.

Online supplemental material

Fig. S1 demonstrates that phosphorylation of Bim1p by Ipl1p is dependent on the presence of Sli15p. Fig. S2 shows GST pull-down assays mapping the interaction of different Bim1 variants with Ipl1p and Sli15p. Fig. S3 documents a potential conformational change in Bim1p upon phosphorylation by Ipl1–Sli15. Fig. S4 shows SEC profiles of full-length and monomeric Bim1 variants. Fig. S5 shows SEC of Bim1 variants fused to EGFP. Videos 1 and 2 show plus end tracking of full-length Bim1-EGFP in vitro visualized by TIRF microscopy. Video 3 shows the behavior of the monomeric Bim1-EGFP protein. Video 4 shows the removal of Bim1–Alexa Fluor 488 from taxol-stabilized MTs upon phosphorylation by Ipl1–Sli15. Video 5 illustrates the release of Bim1-EGFP from dynamic MT ends upon phosphorylation. Video 6 is a live cell Deltavision video showing the behavior of $Bim1^{WT}$–3× GFP during spindle disassembly. Videos 7 and 8 show the behavior of nonphosphorylatable $Bim1^{6A}$–3× GFP during spindle disassembly. Video 9 shows the behavior of the phosphomimicking $Bim1^{6D}$–3× GFP mutant. Online supplemental material is available at http://www.jcb.org/cgi/content/full/jcb.200901036/DC1.

We wish to thank all members of the Westermann laboratory for discussions and Jan-Michael Peters, Tim Clausen, and Peggy Stolt-Bergner for critical reading of the manuscript.

Research in the laboratory of S. Westermann was supported by the European Research Council (ERC) under the European Community's Seventh Framework Program (grant FP7/2007-2013)/ERC starting grant (agreement number 203499) and by the Austrian Science Fund FWF (grant SFB F34-B03).

Submitted: 9 January 2009
Accepted: 9 July 2009

References

Akhmanova, A., and C.C. Hoogenraad. 2005. Microtubule plus-end-tracking proteins: mechanisms and functions. *Curr. Opin. Cell Biol.* 17:47–54.

Akhmanova, A., and M.O. Steinmetz. 2008. Tracking the ends: a dynamic protein network controls the fate of microtubule tips. *Nat. Rev. Mol. Cell Biol.* 9:309–322.

Bieling, P., L. Laan, H. Schek, E.L. Munteanu, L. Sandblad, M. Dogterom, D. Brunner, and T. Surrey. 2007. Reconstitution of a microtubule plus-end tracking system in vitro. *Nature*. 450:1100–1105.

Bieling, P., S. Kandels-Lewis, I.A. Telley, J. van Dijk, C. Janke, and T. Surrey. 2008. CLIP-170 tracks growing microtubule ends by dynamically recognizing composite EB1/tubulin-binding sites. *J. Cell Biol.* 183:1223–1233.

Buvelot, S., S.Y. Tatsutani, D. Vermaak, and S. Biggins. 2003. The budding yeast Ipl1/Aurora protein kinase regulates mitotic spindle disassembly. *J. Cell Biol.* 160:329–339.

Cheeseman, I.M., and A. Desai. 2008. Molecular architecture of the kinetochore-microtubule interface. *Nat. Rev. Mol. Cell Biol.* 9:33–46.

Cheeseman, I.M., C. Brew, M. Wolyniak, A. Desai, S. Anderson, N. Muster, J.R. Yates, T.C. Huffaker, D.G. Drubin, and G. Barnes. 2001. Implication of a novel multiprotein Dam1p complex in outer kinetochore function. *J. Cell Biol.* 155:1137–1145.

Cheeseman, I.M., S. Anderson, M. Jwa, E.M. Green, J. Kang, J.R. Yates III, C.S. Chan, D.G. Drubin, and G. Barnes. 2002. Phospho-regulation of kinetochore-microtubule attachments by the Aurora kinase Ipl1p. *Cell*. 111:163–172.

Cheeseman, I.M., J.S. Chappie, E.M. Wilson-Kubalek, and A. Desai. 2006. The conserved KMN network constitutes the core microtubule-binding site of the kinetochore. *Cell*. 127:983–997.

Ciferri, C., S. Pasqualato, E. Screpanti, G. Varetti, S. Santaguida, G. Dos Reis, A. Maiolica, J. Polka, J.G. De Luca, P. De Wulf, et al. 2008. Implications for kinetochore-microtubule attachment from the structure of an engineered Ndc80 complex. *Cell*. 133:427–439.

des Georges, A., M. Katsuki, D.R. Drummond, M. Osei, R.A. Cross, and L.A. Amos. 2008. Mal3, the *Schizosaccharomyces pombe* homolog of EB1, changes the microtubule lattice. *Nat. Struct. Mol. Biol.* 15:1102–1108.

Gardner, M.K., J. Haase, K. Mythreye, J.N. Molk, M. Anderson, A.P. Joglekar, E.T. O'Toole, M. Winey, E.D. Salmon, D.J. Odde, and K. Bloom. 2008. The microtubule-based motor Kar3 and plus end-binding protein Bim1 provide structural support for the anaphase spindle. *J. Cell Biol.* 180:91–100.

Guimaraes, G.J., Y. Dong, B.F. McEwen, and J.G. Deluca. 2008. Kinetochore-microtubule attachment relies on the disordered N-terminal tail domain of Hec1. *Curr. Biol.* 18:1778–1784.

Hayashi, I., and M. Ikura. 2003. Crystal structure of the amino-terminal microtubule-binding domain of end-binding protein 1 (EB1). *J. Biol. Chem.* 278:36430–36434.

Hayashi, I., A. Wilde, T.K. Mal, and M. Ikura. 2005. Structural basis for the activation of microtubule assembly by the EB1 and p150Glued complex. *Mol. Cell*. 19:449–460.

Honnappa, S., C.M. John, D. Kostrewa, F.K. Winkler, and M.O. Steinmetz. 2005. Structural insights into the EB1-APC interaction. *EMBO J.* 24:261–269.

Hwang, E., J. Kusch, Y. Barral, and T.C. Huffaker. 2003. Spindle orientation in *Saccharomyces cerevisiae* depends on the transport of microtubule ends along polarized actin cables. *J. Cell Biol.* 161:483–488.

Khmelinskii, A., C. Lawrence, J. Roostalu, and E. Schiebel. 2007. Cdc14-regulated midzone assembly controls anaphase B. *J. Cell Biol.* 177:981–993.

Kinoshita, E., E. Kinoshita-Kikuta, K. Takiyama, and T. Koike. 2006. Phosphate-binding tag, a new tool to visualize phosphorylated proteins. *Mol. Cell. Proteomics*. 5:749–757.

Komarova, Y., C.O. De Groot, I. Grigoriev, S.M. Gouveia, E.L. Munteanu, J.M. Schober, S. Honnappa, R.M. Buey, C.C. Hoogenraad, M. Dogterom, et al. 2009. Mammalian end binding proteins control persistent microtubule growth. *J. Cell Biol.* 184:691–706.

Kotwaliwale, C.V., S.B. Frei, B.M. Stern, and S. Biggins. 2007. A pathway containing the Ipl1/aurora protein kinase and the spindle midzone protein Ase1 regulates yeast spindle assembly. *Dev. Cell*. 13:433–445.

Lansbergen, G., and A. Akhmanova. 2006. Microtubule plus end: a hub of cellular activities. *Traffic*. 7:499–507.

Miller, S.A., M.L. Johnson, and P.T. Stukenberg. 2008. Kinetochore attachments require an interaction between unstructured tails on microtubules and Ndc80(Hec1). *Curr. Biol.* 18:1785–1791.

Norden, C., M. Mendoza, J. Dobbelaere, C.V. Kotwaliwale, S. Biggins, and Y. Barral. 2006. The NoCut pathway links completion of cytokinesis to spindle midzone function to prevent chromosome breakage. *Cell*. 125:85–98.

Sandblad, L., K.E. Busch, P. Tittmann, H. Gross, D. Brunner, and A. Hoenger. 2006. The *Schizosaccharomyces pombe* EB1 homolog Mal3p binds and stabilizes the microtubule lattice seam. *Cell*. 127:1415–1424.

Serber, Z., and J.E. Ferrell Jr. 2007. Tuning bulk electrostatics to regulate protein function. *Cell*. 128:441–444.

Slep, K.C., and R.D. Vale. 2007. Structural basis of microtubule plus end tracking by XMAP215, CLIP-170, and EB1. *Mol. Cell*. 27:976–991.

Slep, K.C., S.L. Rogers, S.L. Elliott, H. Ohkura, P.A. Kolodziej, and R.D. Vale. 2005. Structural determinants for EB1-mediated recruitment of APC and spectraplakins to the microtubule plus end. *J. Cell Biol.* 168:587–598.

Sun, L., J. Gao, X. Dong, M. Liu, D. Li, X. Shi, J.T. Dong, X. Lu, C. Liu, and J. Zhou. 2008. EB1 promotes Aurora-B kinase activity through blocking its inactivation by protein phosphatase 2A. *Proc. Natl. Acad. Sci. USA*. 105:7153–7158.

Tanaka, T.U., and A. Desai. 2008. Kinetochore-microtubule interactions: the means to the end. *Curr. Opin. Cell Biol.* 20:53–63.

Tanaka, T.U., M.J. Stark, and K. Tanaka. 2005. Kinetochore capture and bi-orientation on the mitotic spindle. *Nat. Rev. Mol. Cell Biol.* 6:929–942.

Vaughan, K.T. 2005. TIP maker and TIP marker; EB1 as a master controller of microtubule plus ends. *J. Cell Biol.* 171:197–200.

Vitre, B., F.M. Coquelle, C. Heichette, C. Garnier, D. Chrétien, and I. Arnal. 2008. EB1 regulates microtubule dynamics and tubulin sheet closure in vitro. *Nat. Cell Biol.* 10:415–421.

Wei, R.R., J. Al-Bassam, and S.C. Harrison. 2007. The Ndc80/HEC1 complex is a contact point for kinetochore-microtubule attachment. *Nat. Struct. Mol. Biol.* 14:54–59.

Westermann, S., H.W. Wang, A. Avila-Sakar, D.G. Drubin, E. Nogales, and G. Barnes. 2006. The Dam1 kinetochore ring complex moves processively on depolymerizing microtubule ends. *Nature*. 440:565–569.

Westermann, S., D.G. Drubin, and G. Barnes. 2007. Structures and functions of yeast kinetochore complexes. *Annu. Rev. Biochem.* 76:563–591.

Wilson-Kubalek, E.M., I.M. Cheeseman, C. Yoshioka, A. Desai, and R.A. Milligan. 2008. Orientation and structure of the Ndc80 complex on the microtubule lattice. *J. Cell Biol.* 182:1055–1061.

Wong, J., Y. Nakajima, S. Westermann, C. Shang, J.S. Kang, C. Goodner, P. Houshmand, S. Fields, C.S. Chan, D. Drubin, et al. 2007. A protein interaction map of the mitotic spindle. *Mol. Biol. Cell*. 18:3800–3809.